Cellulose
https://doi.org/10.1007/s10570-018-1854-8

COMMUNICATION

# Preparation of cellulose nanofibrils for imaging purposes: comparison of liquid cryogens for rapid vitrification

**Jonathan Ø. Torstensen · Per-Olav Johnsen · Henrik Riis · Richard J. Spontak · Liyuan Deng · Øyvind W. Gregersen · Kristin Syverud**

Received: 12 January 2018 / Accepted: 16 May 2018


**Abstract** Artifact-free imaging of cellulose nanofibrils (CNFs) from aqueous nanocellulose suspensions is nontrivial due to frequent irreversible agglomeration and structure damage during the course of sample preparation, especially as water is solidified prior to freeze-drying. In this study, we have examined the morphologies of CNF suspensions prepared by rapid vitrification in two different liquid cryogens—nitrogen and ethane—followed by freeze-drying. Results obtained by scanning electron microscopy confirm that vitrification in liquid ethane not only greatly improves the survivability of fine-scale CNF structural elements but also significantly reduces the propensity for CNF to agglomerate.

J. Ø. Torstensen · L. Deng · Ø. W. Gregersen · K. Syverud
Department of Chemical Engineering, Norwegian University of Science and Technology (NTNU), 7491 Trondheim, Norway

P.-O. Johnsen · K. Syverud (✉)
RISE- PFI, 7491 Trondheim, Norway
e-mail: kristin.syverud@rise-pfi.no

H. Riis
Department of Physics, University of Oslo, 0315 Oslo, Norway

R. J. Spontak
Departments of Chemical and Biomolecular Engineering and Materials Science and Engineering, North Carolina State University, Raleigh, NC 27695, USA

**Keywords** Nanocellulose · Cellulose nanofibril · Freeze-drying · Cryopreparation · Scanning electron microscopy

## Introduction

A recurring issue concerning the morphological characterization of nanocellulose, such as cellulose nanofibrils (CNFs), is selecting specimen preparation techniques that preclude both agglomeration and structural damage prior to imaging and specific surface area measurement (Peng et al. 2012). This consideration likewise extends to drying nanocellulose for subsequent re-dispersion (Liu et al. 2018). While ensuring retention of "never-dried" CNF and its virgin structure is not yet fully achievable, several preparation protocols have been developed for use in conjunction with scanning electron microscopy (SEM) and specific surface area measurements. Of these, the most common are freeze-drying, usually performed with liquid nitrogen as the vitrification cryogen, and critical-point drying, previously conducted with fluorinated volatile organic compounds but now restricted largely to carbon dioxide. In the former, a crucial consideration is that vitrification (the formation of a glassy solid) and not crystallization (due to freezing in the thermodynamic sense) must be achieved to minimize, if not altogether avoid, the formation of





Journal : Medium 10570 | Dispatch : 30-5-2018 | Pages : 6
Article No. : 1854 | ☐ LE | ☐ TYPESET
MS Code : CELS-D-18-00032 | ☑ CP | ☑ DISK

morphology-damaging crystals. For this reason, a consistent and undesirable problem associated with liquid nitrogen is the undesirable production of artefactual CNF agglomerates.

Freezing can generally be described by the Biot number (Bi) (Bailey and Zasadzinski 1991), which is given by

$$Bi = \frac{hV}{kA} \quad (1)$$

where $h$ represents the heat transfer coefficient associated with the heat transferred across an interface between, for instance, a liquid and a sample of known cross-section, $k$ is the heat transfer coefficient of the sample, and $V$ and $A$ denote the sample volume and surface area, respectively. Preparation of samples by cryogenic methodologies requires $V \ll A$ to guarantee uniform freezing. Moreover, the freezing rate of the liquid cryogen is also determined by the phase behavior of the freezing liquid. In the case of liquid nitrogen, the cooling rate is inhibited by the Leidenfrost effect, which relates to the formation of an insulating vapor layer between the sample and cooling medium at the normal boiling point of the liquid cryogen. Because of the formation of this layer that severely hinders heat transfer, reducing $h$ in Eq. (1). The cooling rate of liquid nitrogen is at most only $\sim$ 560 °C/s (Ryan 1992). This shortcoming is greatly enhanced in cryogenic transmission electron microscopy (cryo-TEM) wherein poor heat transfer results in the formation of hexatic ice crystals that dramatically damage the existing morphologies of colloidal or biological nanostructures dispersed in a liquid matrix.

A long-standing solution developed to overcome this technical challenge for cryo-TEM relies on using liquid nitrogen to cool ethane from gas to liquid to solid (Echlin 1992), since the normal boiling point of nitrogen is − 196 °C whereas the normal boiling and freezing points of ethane are − 88.5 and − 182 °C, respectively. During specimen preparation, however, the solid ethane can be warmed slightly (by, for example, direct contact with a heat sink) so as to liquefy, and the resultant supercooled liquid exhibits a significantly reduced Leidenfrost effect with virtually no insulating vapor boundary layer. Cooling rates realized in supercooled liquid ethane are much greater, typically 0.3–1.6 $\times$ $10^4$ °C/s, depending on sample geometry and the vitrification configuration (Bailey and Zasadzinski 1991; Ryan 1992). The cooling rate of liquid ethane is therefore more than an order of magnitude greater than that of conventional liquid nitrogen. It can actually be significantly higher ($\sim$ 100 $\times$), since the cooling rate of liquid nitrogen has been reported as low as 80 °C/s (Bailey and Zasadzinski 1991). Since ethane is highly flammable, caution must be exercised in using liquid ethane.

While this methodology has been previously employed (Frey et al. 1996) to study the detailed morphology of cellulose gels containing ammonia/ammonium thiocyanate as the solvent, the present study focuses on the preparation of CNF suspensions for SEM imaging. Due to their fine structure, freezing in the thermodynamic sense will lead to the formation of ice crystals that will deleteriously affect the CNF morphology. In this case, the vitrification of water is crucial to minimize the extent of crystal-induced artifacts. One such example is the nontrivial reduction in available CNF space due to the formation of ice crystals that expand as they undergo nucleation and growth. In this case, suspended CNF is pushed together between crystals, which leads to agglomeration. A high freezing rate during cooling likewise decreases the size of ice crystals range from $\sim$ 1 μm (Dubochet et al. 1982) in liquid nitrogen to 30–50 nm in liquid ethane (Ryan et al. 1990). This consideration explains why agglomeration is so prominent when samples are solidified in liquid nitrogen. The objective of this study is to compare the morphological features of CNF suspensions vitrified by both cryogens and discern the effect of cooling on the extent of CNF agglomeration. Our ultimate goal is to present a straightforward sample preparation method that preserves the 3D network structure CNF is known to form. Typical approaches are AFM (Jiang and Hsieh 2013; Heggset et al. 2017; Moberg et al. 2017) or TEM with uranyl acetate (Saito et al. 2007) or without staining (Deepa et al. 2015). While these techniques are valuable, they typically image individual fibrils and do not capture the 3D network which is clearly seen using liquid ethane in this paper.

## Materials and methods

### Materials

In this study, CNF obtained from cellulose pulp and surface-oxidized with 2,2,6,6-tetramethyl-piperidin-1-yl)oxyl (TEMPO) was used. Two types of CNF were examined, one with a low surface charge of





Journal : Medium 10570 | Dispatch : 30-5-2018 | Pages : 6
Article No. : 1854 | LE | TYPESET
MS Code : CELS-D-18-00032 | CP | DISK

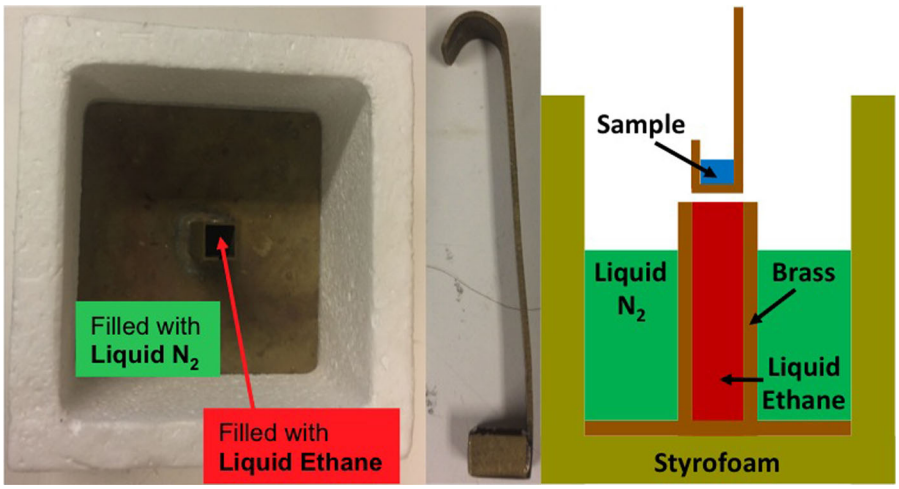


**Fig. 1** (left) Photograph of the experimental set-up used for rapid vitrification. The styrofoam box and brass chamber are evident. (middle) The brass specimen holder used to contain the aqueous CNF suspension. (right) Schematic illustration of the cross-section of the set-up

716 ± 20 μmol/g (L-CNF) and the other with a higher surface charge of 958 ± 15 μmol/g (H-CNF), as determined by conductiometric measurements (Saito and Isogai 2004). Details of the oxidation reaction are provided elsewhere (Ø Torstensen et al. 2018). The final amounts of included NaClO were 2 mmol/g pulp (L-CNF) or 3.28 mmol/g pulp (H-CNF), wherein the NaClO was added as 12.7 mmol/min to 120 g of pulp.

## Methods

The same specimen vitrification set-up was used for both liquid cryogens and consisted of an insulating styrofoam box outfitted with a small hollow brass chamber inside, as displayed in Fig. 1. In the case of using liquid nitrogen as the cryogen, both the styrofoam box and brass chamber were filled with liquid

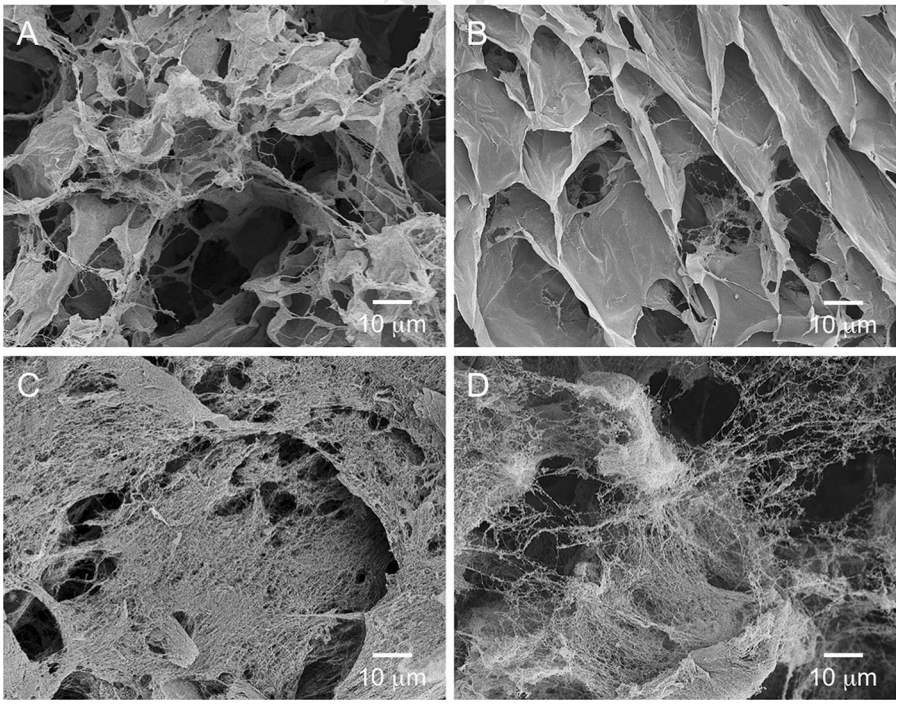


**Fig. 2** SEM images acquired from aqueous CNF suspensions composed of 0.8 wt% CNF and rapidly vitrified in two different liquid cryogens—liquid nitrogen (**a**, **b**) and liquid ethane (**c**, **d**)—for L-CNF (**a**, **c**) and H-CNF (**b**, **d**)



Journal : Medium 10570 | Dispatch : 30-5-2018 | Pages : 6
Article No. : 1854 | ☐ LE | ☐ TYPESET
MS Code : CELS-D-18-00032 | ☑ CP | ☑ DISK

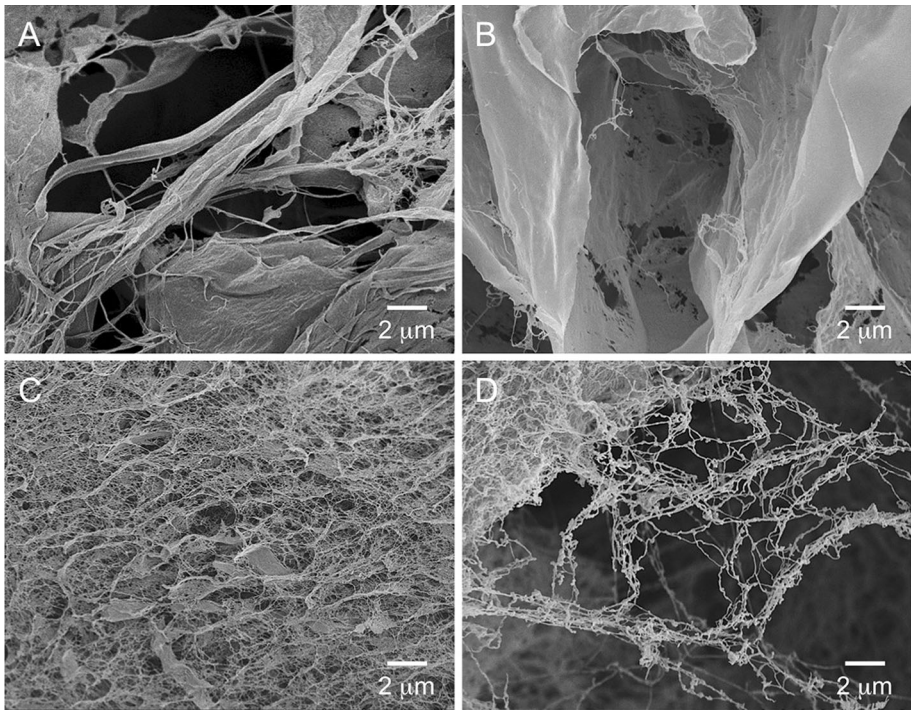


**Fig. 3** SEM images collected at higher resolution than those in Fig. 2 from aqueous CNF suspensions composed of 0.8 wt% CNF and rapidly vitrified in two different liquid cryogens—liquid nitrogen (**a**, **b**) and liquid ethane (**c**, **d**)—for L-CNF (**a**, **c**) and H-CNF (**b**, **d**)

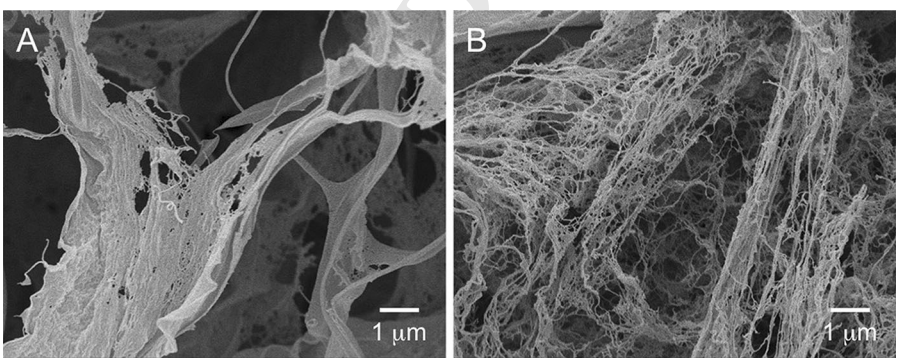


**Fig. 4** SEM images acquired from aqueous CNF suspensions composed of 0.8 wt% L-CNF and rapidly vitrified in two different liquid cryogens: liquid nitrogen (**a**) and liquid ethane (**b**)

nitrogen, and the specimen was quickly immersed by hand, as described below. Substitution of liquid ethane as the cryogen was more complicated. The styrofoam box was filled with liquid nitrogen and allowed to stabilize beyond nucleic boiling so that it could cool the brass chamber down to − 196 °C. As mentioned earlier, ethane gas (purity 99.5%, AGA, Oslo, Norway) was introduced into the empty brass chamber. Since the melting point of ethane is − 182 °C, the gaseous ethane first liquefied and then froze due the external cooling provided by liquid nitrogen. While solid ethane is often returned to its liquid state prior to vitrification by briefly introducing a heat source, our efforts demonstrated that liquid ethane could be retained by simply filling the brass chamber above the liquid nitrogen line. The CNF suspension containing 0.8 wt% CNF in deionized water was first poured into a matched brass specimen holder measuring $0.9 \times 0.9 \times 0.5\ cm^3$ in volume and pictured in Fig. 1. The specimen holder was quickly inserted into



Journal : Medium 10570 | Dispatch : 30-5-2018 | Pages : 6
Article No. : 1854 | ☐ LE | ☐ TYPESET
MS Code : CELS-D-18-00032 | ☑ CP | ☑ DISK

**Table 1** Nanofibril widths measured for two different types of CNF rapidly vitrified using either liquid nitrogen or liquid ethane

| L-CNF | | H-CNF | |
|---|---|---|---|
| Liquid $N_2$ | Liquid ethane | Liquid $N_2$ | Liquid ethane |
| 91.3 ± 40.0 nm | 66.3 ± 19.0 nm | 85.2 ± 24.8 nm | 93.0 ± 27.1 nm |

the chamber, paying careful attention to avoid having the holder touch the chamber walls (which could result in adherence). Once CNF specimens were vitrified in either cryogen, they were removed from the chamber and samples were inserted into the freeze dryer in a bath of liquid nitrogen. In the freeze drying unit (Biobase BK-FD12/Heto CT 60e) water was sublimed by freeze-drying at 33 Pa for a minimum of 16 h. After freeze-drying, the specimens were carefully removed from the holder (since they were very fragile and easily fractured), placed on Al stubs and sputter-coated with 15 nm of Au to avoid charging during characterization. Secondary-electron SEM images of fracture surfaces were acquired on a Hitachi SU3500 microscope operated at 5 kV. Fibril widths were measured manually in FIJI (ImageJ). Each nanofibril diameter measurement employed a line measuring 5 pixels across. Measurements were collected from at least two different sample areas for each specimen, and sampling numbers ranged from 400 for L-CNF to 600 for H-CNF.

## Results and discussion

According to independent studies (Fujisawa et al. 2011; Rodionova et al. 2013), TEMPO-oxidized CNFs possess a width of 1.6–4.0 nm. Typical SEM images acquired from the CNF suspensions by both specimen preparation routes described above are displayed for comparison in Figs. 2, 3 and 4. The liquid-ethane preparation method was repeated twice for H-CNF, yielding the same type of sample morphology both times. The artefactual honeycomb structure that is commonly observed (Jiang and Hsieh 2014) when freeze-drying CNF after exposure to liquid nitrogen due to water crystallization is not nearly as prominent in the specimen vitrified in liquid ethane (cf. Figure 2). Moreover, L-CNF appears to exhibit slightly less honeycomb structure relative to H-CNF when quenched in liquid $N_2$. Further comparison at higher spatial resolution in Figs. 3 and 4 more clearly reveals the influence of vitrification cryogen on resultant morphology. Although the artefactual honeycomb structure can still be observed, individual fibrils are evident in all sample types. Analysis of SEM images confirms that the thinnest discernible CNF nanofibrils consistently measure 60–100 nm across (cf. Table 1) and are therefore agglomerations of individual cellulose nanofibrils. These measurements are not performed on regions that display sheet-like or honeycomb structures. These measurements clearly do not quantitatively reflect the morphologies of specimens rapidly vitrified in liquid nitrogen in Fig. 2a, b.

We propose that future morphological studies of CNF suspensions adhere to a specimen protocol wherein liquid ethane is employed as the rapid vitrification cryogen prior to freeze-drying. The results reported here unequivocally establish that more representative morphological details of CNF suspensions can be retained in bulk specimens through the use of liquid ethane. Apart from being important with respect to imaging the representative CNF morphology, it will also have a significant impact on other metrics such as the specific surface area (Jiang and Hsieh 2014).

**Acknowledgments** This work was supported by the Research Counsel of Norway through the NANO 2021 program (Grant Number 239172) and NANO-MBE projects. We are grateful to I. Leirset and A. Reitan for technical assistance and to Sødra for supplying the pulp.

## References

Bailey SM, Zasadzinski JAN (1991) Validation of convection-limited cooling of samples for freeze-fracture electron microscopy. J Microsc 163:307–320

Deepa B, Abraham E, Cordeiro N, Mozetic M, Mathew AP, Oksman K, Faria M, Thomas S, Pothan LA (2015) Utilization of various lignocellulosic biomass for the production of nanocellulose: a comparative study. Cellulose 22:1075–1090





Journal : Medium 10570 | Dispatch : 30-5-2018 | Pages : 6
Article No. : 1854 | LE | TYPESET
MS Code : CELS-D-18-00032 | CP | DISK

Dubochet J, Lepault J, Freeman R, Berriman J, Homo J (1982) Electron microscopy of frozen water and aqueous solutions. J Microsc 128:219–237

Echlin P (1992) Low-temperature microscopy and analysis. Springer, New York

Frey MW, Cuculo JA, Spontak RJ (1996) Morphological characteristics of the lyotropic and gel phases in the cellulose/NH3/NH4SCN system. J Polym Sci, Part B: Polym Phys 34:2049–2058

Fujisawa S, Okita Y, Fukuzumi H, Saito T, Isogai A (2011) Preparation and characterization of TEMPO-oxidized cellulose nanofibril films with free carboxyl groups. Carbohydr Polym 84:579–583

Heggset EB, Chinga-Carrasco G, Syverud K (2017) Temperature stability of nanocellulose dispersions. Carbohydr Polym 157:114–121

Jiang F, Hsieh Y-L (2013) Chemically and mechanically isolated nanocellulose and their self-assembled structures. Carbohydr Polym 95:32–40

Jiang F, Hsieh Y-L (2014) Super water absorbing and shape memory nanocellulose aerogels from TEMPO-oxidized cellulose nanofibrils via cyclic freezing–thawing. J Mater Chem A 2:350–359

Liu Y, Stoeckel D, Gordeyeva K, Agthe M, Schütz C, Fall AB, Bergström L (2018) Nanoscale assembly of cellulose nanocrystals during drying and redispersion. ACS Macro Lett 7:172–177

Moberg T, Sahlin K, Yao K, Geng S, Westman G, Zhou Q, Oksman K, Righdal M (2017) Rheological properties of nanocellulose suspensions: effects of fibril/particle dimensions and surface characteristics. Cellulose 24:2499–2510

Peng Y, Gardner DJ, Han Y (2012) Drying cellulose nanofibrils: in search of a suitable method. Cellulose 19:91–102

Rodionova G, Saito T, Lenes M, Eriksen Ø, Gregersen ØW, Kuramae R, Isogai A (2013) TEMPO-mediated oxidation of norway spruce and eucalyptus pulps: preparation and characterization of nanofibers and nanofiber dispersions. J Polym Environ 21:207–214

Ryan KP (1992) Cryofixation of tissues for electron microscopy: a review of plunge cooling methods. Scanning Microsc 6:715–743

Ryan KP, Bald WB, Neumann K, Simonsberger P, Purse DH, Nicholson DN (1990) Cooling rate and ice-crystal measurement in biological specimens plunged into liquid ethane, propane, and Freon 22. J Microsc 158:365–378

Saito T, Isogai A (2004) TEMPO-mediated oxidation of native cellulose. The effect of oxidation conditions on chemical and crystal structures of the water-insoluble fractions. Biomacromolecules 5:1983–1989

Saito T, Kimura S, Nishiyama Y, Isogai A (2007) Cellulose nanofibers prepared by TEMPO-mediated oxidation of native cellulose. Biomacromolecules 8:2485–2491

Torstensen JØ, Liu M, Jin S-A, Deng L, Hawari AI, Syverud K, Spontak RJ, Gregersen ØW (2018) Swelling and free-volume characteristics of TEMPO-oxidized cellulose nanofibril films. Biomacromolecules 19:1016–1025





Journal : Medium 10570 | Dispatch : 30-5-2018 | Pages : 6
Article No. : 1854 | ☐ LE | ☐ TYPESET
MS Code : CELS-D-18-00032 | ☑ CP | ☑ DISK